Granular Matter
DOI 10.1007/s10035-012-0370-z

PUBLISHER'S ERRATUM

Erratum to: Investigating the micromechanical evolutions within inherently anisotropic granular materials using discrete element method

Ehsan Seyedi Hosseininia

Erratum to: Granular Matter
DOI 10.1007/s10035-012-0340-5

Owing to an unfortunate technical error, this article appeared with an incorrect year of publication in the credit line, which was given as "Granular Matter (2007) 14:483–503". The correct credit line is as follows:

Granular Matter (2012) 14:483–503

The publisher sincerely apologizes for this mistake.

The online version of the original article can be found under doi:10.1007/s10035-012-0340-5.

E. Seyedi Hosseininia (✉)
Civil Engineering Department, Faculty of Engineering, Ferdowsi University of Mashhad, P.O. Box: 91775-1111, Mashhad, Iran
e-mail: eseyedi@um.ac.ir

Published online: 25 August 2012

Granular Matter (2007) 14:483–503
DOI 10.1007/s10035-012-0340-5

ORIGINAL PAPER

Investigating the micromechanical evolutions within inherently anisotropic granular materials using discrete element method

Ehsan Seyedi Hosseininia

Received: 25 September 2011 / Published online: 17 March 2012

Abstract This paper investigates the mechanical behavior of inherently-anisotropic granular materials from macroscopic and microscopic points of view. The study is achieved by simulating biaxial compression tests performed on granular assemblies by using numerical discrete element method. In the same category of numerical studies found in the literature, the simulations were performed by considering elliptical/oval particles. In the present study, however, the shape of particles is considered as convex polygons, which mostly resembles real sand grains. Particle assemblies with four different bedding angles were tested. Similar to what observed in experiment, inherent anisotropy has a significant effect on macroscopic mechanical behavior of granular materials. The shear strength and dilative behavior of assemblies were found to decrease as the bedding angle increases. Evolution of the microstructure of all samples and the influence of bedding angle on the fabric and force anisotropy during loading process were investigated. It is seen that the microscopic evolutions in the fabric can justify well the macroscopic behavior of granular assemblies. It is found that the long axis of particles tend to be inclined perpendicular to the loading axis, which results in generating more stable column-like microstructures in order to transfer the applied load. Moreover, the number of contacts as well as the magnitude of forces among particles varies in different directions during the loading process and the initial anisotropy condition totally evolves due to the induced anisotropy within samples.

Keywords Discrete elements · Simulation · Micro mechanics · Granular media · Mechanical properties · Anisotropy

E. Seyedi Hosseininia (✉)
Civil Engineering Department, Faculty of Engineering,
Ferdowsi University of Mashhad, P.O. Box: 91775-1111, Mashhad, Iran
e-mail: eseyedi@um.ac.ir

1 Introduction

Anisotropy is a common phenomenon in a granular material since it consists of individual discrete bodies. There are many studies suggested that the anisotropy is one of the most important aspects to be taken into account for better understanding of the mechanics of granular soils [1–7]. The first type of anisotropy in granular materials especially in naturally deposited sands is inherent anisotropy. It pertains to the initial spatial arrangement of particles, voids, and associated contacts. This is generally initiated during the deposition of soil particles under gravity so that the long axis of particles tends to align in a specific direction, which is termed as bedding plane. Such initially-generated structure in granular materials influences the mechanical behavior including shear strength and deformability, which is an important issue in geotechnical engineering problems. There exists another type of anisotropy, which occurs during loading process and shear deformation of aggregate media. The latter is referred to induced anisotropy. In fact, the anisotropy induced in the fabric explains variations observed in the mechanical response of granular materials. Such fabric evolution is also affected by the inherent anisotropy in the medium.

Studying the mechanical behavior of inherently anisotropic granular soils have been the subject of many experimental/laboratorial researches. Different test methods including plane strain compression tests [8–11], direct shear tests [5,12], triaxial tests [8,13], true triaxial tests [14,15], and hollow cylinder torsion shear tests [9,15,16] have been used to find characteristics of initially anisotropic sand fabrics. In addition to the efforts made by testing on naturally deposited and laboratory-prepared sand samples, biaxial compression tests were also performed by using two-dimensional assemblies of photo-elastic oval cross-sectional rods [17]. The outcome of all these tests wholly indicates that shear strength

and deformability of granular soils is highly dependent on the initial fabric condition. In other words, the stress-strain behavior of such soils significantly varies with the direction of applied loading or stresses with respect to the bedding plane.

Regardless of the initial condition within the soil fabric, an evolution in the soil fabric occurs when a granular soil undergoes shear deformation. The evolution in fabric corresponds to the changes in particle arrangement as well as development/disappearance of contacts between particles. A remarkable aspect of such induced anisotropy is the development of vertical columns through which the major principal stress is transmitted. Wakabayashi [18] and Drescher [19] observed dark bands in stressed assemblies of optically sensitive particles under polarizing light and interpreted them as principal stress trajectories. The same experience was obtained by Oda et al. [17] by using photo-elastically sensitive rod-like particles in biaxial compression tests. The particles had oval cross sections. They found that during the sample deformation and up to the peak stress ratio, new contacts are continually generated in such a manner that they tend to concentrate more in the direction parallel to the major principal stress axis. This concentration seems to be closely related to the formation of new column-like load paths which carry the increasing applied stress in that direction. After the peak stress ratio, however, buckling of such column-like microstructures occurs, but considerable rearrangement of the load paths takes place and new concentrations lead to form new columns. Therefore, the generation and collapse of columns carries on successively. The other observation in their test was the appearance of large voids between the buckling columns. They explained that such happening is the reason why large dilatancy can be found after the peak stress [17]. Oda et al. [20] compared these results with those of plane strain tests on Ticino and Toyoura sands [21] and they found that the same happenings can take place in real sand samples within narrow shear bands. Accordingly, it is possible to say that the mechanical behavior of granular materials can be well interpreted as a consequence of microscopic events within the assembly.

The numerical discrete element method (DEM) has been used increasingly in recent years to investigate the behavior of granular soils both from macro and micromechanical points of view. By using DEM, the mechanical response of granular media can be acquired by considering each particle as an individual body having interactions with its neighboring particles as a dynamic process and using simple mechanical laws for their interactions. In addition, DEM is a very powerful tool in order to study the evolutions taken place in the microstructure of granular materials. For instance, DEM facilitates to investigate the development of stress/force transmission [22,23], contact network [24], and generation of shear zones [25]. In the simplest form, the simulations of aggregates can be performed by circular discs [26–28] or spheres [29,30]. Due to the simplicity in particle shapes, the advantage of these simulations is the reduction in calculation time. However, such simplification has some imperfections. Firstly, these simulations do not consider the effect of particle shape and different dimensions in different directions. Secondly, another shortcoming arises from the excessive freedom of these particles, which causes higher degree of rotation in comparison with real sand particles. There have been various attempts to eliminate this imperfection. Regarding two-dimensional simulations with circular particles, Iwashita and Oda [31,32] introduced modified discrete element method (MDEM), in which the conventional DEM is modified in such a way that the effect of rolling resistance at contact points could be taken into account. By comparing the results of DEM with those of MDEM simulations, they showed that column-like microstructures, large voids and high degree of particle rotation in shear bands can be well obtained by MDEM in quite similar manner to natural sands. A similar approach has been taken into account in simulating 3-D sphere particles [33]. However, MDEM can not be used when it is aimed to study the inherent anisotropy in granular materials, because there is no elongation and preferred orientation in the geometry of circular/spherical particles. As another alternative for the above mentioned imperfection of circular/spherical particles is to use non-circular/non-spherical particles, which are often elliptical/oval in shape and are used in both 2-D [27,34,35] and 3-D simulations [36]. Ideas for creating non-circular/non-spherical particles are clusters of bonded circles/spheres [37] or overlapping rigid clusters [38]. Although these clustering techniques provide non-circular/non-spherical particles for more rigorous simulations, they would require a big amount of memory and thus, the calculation time increases.

The other approach, which will be used in the present study, is to use convex polygon-shaped particles [39,40]. By this approach, it is possible to predefine the geometry of particles in numerical assemblies as arbitrary convex polygons. Each particle is considered as a rigid body in similar manner to simulations with circular/elliptical particles and thus, not only the simulation process is simple and efficient compared to clustering techniques, but also the geometry of particles are very close to real soil particles compared with elliptical particles.

The present paper aims to investigate the evolution of microstructure within two-dimensional inherently anisotropic granular materials. The study is achieved by simulating biaxial compression tests for four series of granular assemblies using DEM. Each sample contains a set of elongated polygon-shaped particles, which makes the results of simulations more reliable compared with using elliptical particles. The state of inherent anisotropy is taken into consideration by generating assemblies in such a way that the average initial

bedding angle of particles is oriented towards a specific direction with respect to the loading axis. The effect of inherent anisotropy on the behavior of assemblies is firstly studied in terms of shear strength as well as deformability. Then, more specifically in this paper, the microstructure evolutions inside the assemblies are investigated by following the rearrangement of contacts and distribution of contact forces during loading process.

2 Principles of the numerical procedure

Numerical simulations are carried out by using DEM. In DEM, a granular material is considered as a group of individual particles and equations of motion are solved for each particle using implicit time integration method. A brief review of the numerical procedure is explained below, which is based on the original work presented by [41].

2.1 Equations of motion

In a Cartesian coordinates system $(x_1 - x_2)$, consider an individual particle surrounded by neighboring particles as shown in Fig. 1a. The particle may have interactions with some of the adjacent particles through the contact points. Consequently, the particle as a rigid body can move and rotate due to applied peripheral forces from adjacent particles (Fig. 1b). The rotational and translational accelerations of motion can be calculated for each particle by using Newton's second law of motion:

$$\begin{aligned} I\ddot{\theta} &= \sum_{c=1}^{N_c} M^c \\ m\ddot{X}_i &= \sum_{c=1}^{N_c} F_i^c \end{aligned} \tag{1}$$

where m and I are the mass and moment of inertia of the particle. F_i^c and M^c are the ith force component $(i = 1, 2)$ and the moment applied at the center of gravity of the particle, respectively. N_c is the number of contacts with other particles. $\ddot{X}_i$ and $\ddot{\theta}$ are translational component and rotational accelerations of the particle, respectively. These equations are integrated once to calculate the respective velocity and then once again to find the displacement components as well as rotation.

In addition to the forces and moments caused by contacts, particles are imposed by extra force and moment components representing viscous damping in order to maintain the stability of the method by dissipating particle movements. To do so, the values of the damping force component F_i^D and the damping moment M^D are related to the translational $(\dot{X}_i)$ and rotational $(\dot{\theta})$ velocity components by constants C_m and C_I as follows:

$$\begin{aligned} F_i^D &= -C_m \dot{X}_i \\ M^D &= -C_I \dot{\theta} \end{aligned} \tag{2}$$

where $C_m = \alpha_m m$ and $C_I = \alpha_I I$, in which α_m and α_I are damping coefficients.

It is noted that the accuracy of such simulation is mainly related to the prediction of interactions between particles. During loading, new contacts may be generated and at the same time, some of existing contacts may be disappeared. As a consequence, the simulation is a dynamic process and equations of motion should be solved for each particle in every time step during the simulation process.

2.2 Contact law

The shape of particles in simulations is considered as convex polygon i.e., having sharp corners and edges and thus,

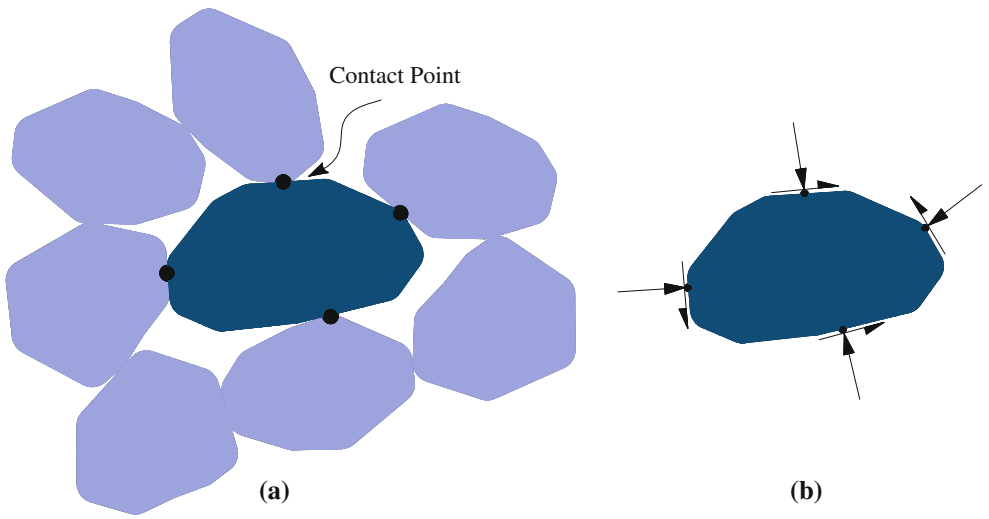

Fig. 1 **a** Presentation of a particle surrounded by neighboring particles; **b** associated contact forces on the particle

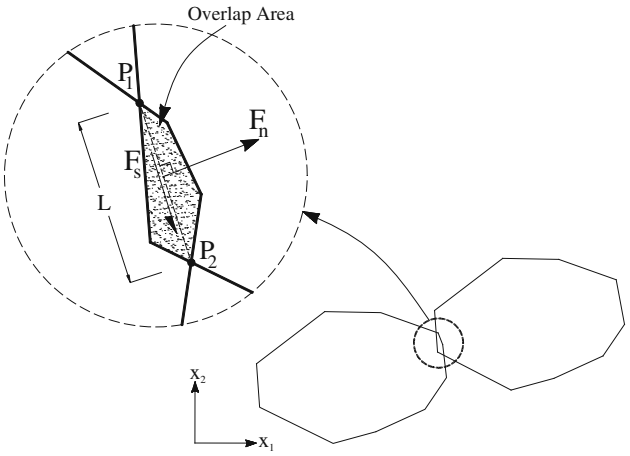

Fig. 2 Representation of contact definition between two angular particles

the contact detection algorithm is the main challenge in the simulation process. Mirghasemi et al. [39] introduced and examined two different contact laws (linear and overlap-area) for angular particles and they showed that both contact laws yield similar results. In the present study, the overlap-area contact law is applied in simulations.

Consider two polygon-shaped particles having contact with each other according to Fig. 2. The contact is characterized by an overlap area between two particles. The line between the intersection points P_1 and P_2 indicates the contact length (L) between particles. The indentation length (δ) can be defined as $\delta = A/L$, where A is the overlap area between particles. The contact force is assumed to be imposed at the middle of the $\overline{P_1P_2}$ line. Each contact force comprises of normal and tangential components. The direction of the normal contact force (F_n) is perpendicular to the line $\overline{P_1P_2}$ and the value is calculated as follows:

$$F_n = k_n \delta \tag{3}$$

where k_n is normal stiffness coefficient. Similarly, the tangential contact force (F_s) exerted along the line $\overline{P_1P_2}$, is defined as:

$$F_s = k_s \Delta \tag{4}$$

where k_s is shear stiffness coefficient and Δ is the relative tangential displacement of two particles along the line $\overline{P_1P_2}$. The relationship between the normal contact force and indentation length (Eq. 3) is elastic. In contrary, it is assumed that the contact surface along the line $\overline{P_1P_2}$ behaves as frictional and the elastic tangential force-displacement relationship is limited. It means that sliding may occur along the contact surface when $|F_s| > \mu_s F_n$. Otherwise, the relationship between shear force and tangential displacement is recoverable. μ_s equals $\tan\phi_\mu$, where ϕ_μ is the inter-particle friction angle, whose value relates to the characteristics of the particles material [42].

2.3 Average stress tensor

In a granular assembly, the average stress tensor (σ_{ij}) can be computed as an average of microscopic characteristics as follows [43,44]:

$$\sigma_{ij} = \frac{1}{V}\sum_{c=1}^{N_c} f_i^c l_j^c \quad i, j = 1, 2 \tag{5}$$

The sum above is with respect to the total number of contacts (N_c) in the volume V. f_i^c is the ith component of the contact force acting at the cth contact point between two particles; l_j^c is the jth component of the contact vector that points from the center of the mass of each particle to the middle of the contact surface.

Alternatively, the average stress tensor can be obtained from tractions applied on the boundary of the assembly. If external forces $T_i^1, T_i^2, \ldots, T_i^m$ are exerted on the boundary points $x_i^1, x_i^2, \ldots, x_i^m$, the average stress tensor of an assembly with statically balanced condition can also be assessed by:

$$\sigma_{ij} = \frac{1}{V}\sum_{b=1}^{m} T_i^b x_j^b \quad i, j = 1, 2 \tag{6}$$

2.4 Average strain tensor

The average strain tensor (ε_{ij}) of an assembly with the volume V can be obtained by measuring displacements of boundary particles [26]:

$$\varepsilon_{ij} = \frac{1}{V}\sum_{\beta=1}^{N_b}\left[\frac{1}{2}\{\Delta x_j^\beta + \Delta x_j^{\beta+1}\} e_i^\beta S^\beta\right] \quad i, j = 1, 2 \tag{7}$$

The boundary is defined by connecting the center of all boundary particles to each other. In accordance with Fig. 3, Δx_j^β and $\Delta x_j^{\beta+1}$ represent the jth component of the two adjacent particles displacement, which are connected to each other through the line S^β. e_i^β is the ith component of the unit vector whose direction is perpendicular to S^β. N_b in the above equation is the number of total boundary contacts.

3 Numerical simulations

The numerical procedures described above have been implemented in a computer program called POLY [39]. It is a developed version of the code DISC [45], which was used to model two-dimensional biaxial compression tests with circular particles. POLY has been later developed for simulating breakage phenomenon in convex angular particles [46].

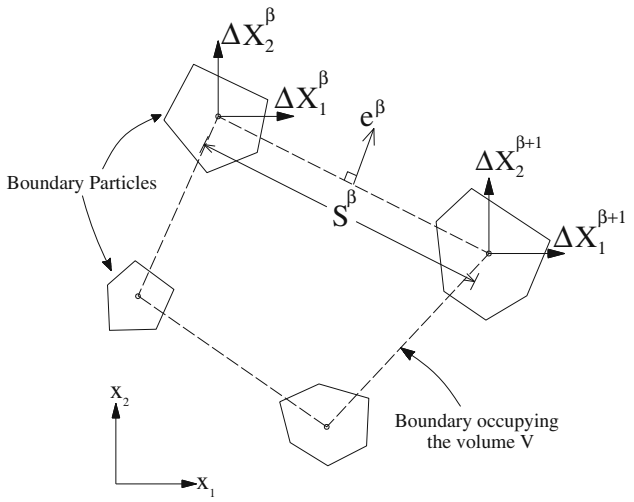

Fig. 3 Definition of the average strain tensor by considering displacements of boundary particles

3.1 Particle generation

As explained before, the particles are considered as polygon in shape. The geometry of each particle as a polygon is defined by introducing the coordinates of the polygon corners. The particle geometry can be considered arbitrarily except for being convex. This condition is because of the contact detection algorithm. It is also possible to define arbitrary number of particle types regarding the size and geometry. In the present study, three forms of elongated particles are chosen with three different sizes. The geometry of the particles is considered in such a way that a particle is surrounded by an ellipse. Accordingly, the major and minor axes of a particle are defined as the long and short axes of the surrounded ellipse, respectively. The orientation of a particle with respect to the horizontal axis is determined by the direction of the major (or long) axis. It is noted that the procedure used for the definition of particle orientation does not directly consider a unique value of the particle orientation related to the particle geometry. Instead, one can use the concept of inertia tensor defined by Pena et al. [47], by which the distribution of mass of particles can be correctly obtained. Consequently, the procedure used in this study to investigate the changes in the orientation of particles is only an approximation and not unique. The similarity between polygon-shaped and elliptical particles is considered intentionally only for comparison of the results with those of simulations with elliptical particles in the literature [48]. The geometry of particles is shown in Fig. 4. The aspect ratio (the ratio of the major axis length to the minor axis length) of all ellipses is 1.5. The particle sizes represented by the major axis length include 4.5, 5.0, and 7.0 mm.

3.2 Fabrication of numerical specimens

In the present study, the specimens have the form of a circular region. This form of specimens originates from the idea that the stress distribution within such geometry would be more uniform compared to the specimens with four-edged regions and thus, stress concentration and/or strain localization inside the assembly is prohibited. Based on the particle size and type distribution introduced for specimens, particles are placed randomly inside the circular region. A particle is laid down inside the region in condition that it has no overlap with previously-laid particles. Furthermore, since inherently anisotropic assemblies are aimed to be prepared, the code is modified to place each particle provided that major axis of the particle be oriented along a pre-defined direction i.e., bedding plane. It is noted that in the literature, there is another numerical technique used to prepare inherently anisotropic samples and that is the pluviation method, which is similar to sand pluviation in real laboratory tests [8,49]. In this method, the gravity force is considered in calculations and thus, a pack of sand is deposited as sediment. It is obvious that the specimen prepared by the pluviation method is very similar to what happens in the nature. However, the simulation process used in this paper is less time-consuming in comparison with the pluviation method. In each specimen, whose diameter is 160 mm, about 2,000 particles can be stacked. The sample diameter is large enough in order to neglect the effect of particle size on test results ($D_{sample}/D_{particle} \approx 21$).

A scheme of the four initially-generated samples with bedding plane of $\alpha = 0°, 30°, 60°,$ and $90°$ with respect to the horizontal is depicted in Fig. 5. At the initial state of the sample generation, particles are sparsely positioned inside the circular region. In order to reduce the gaps between particles and make the specimens denser, an initial isotropic

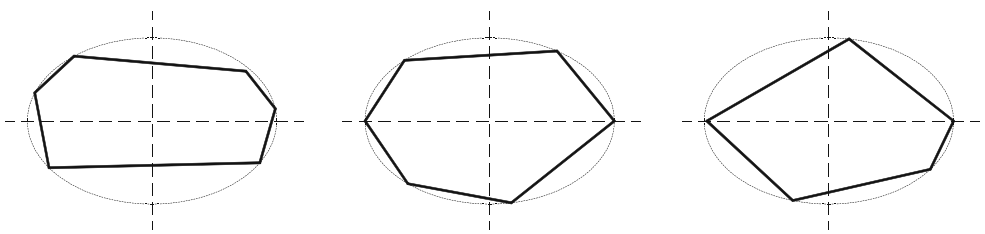

Fig. 4 Schematics of the geometry of particles used in simulations

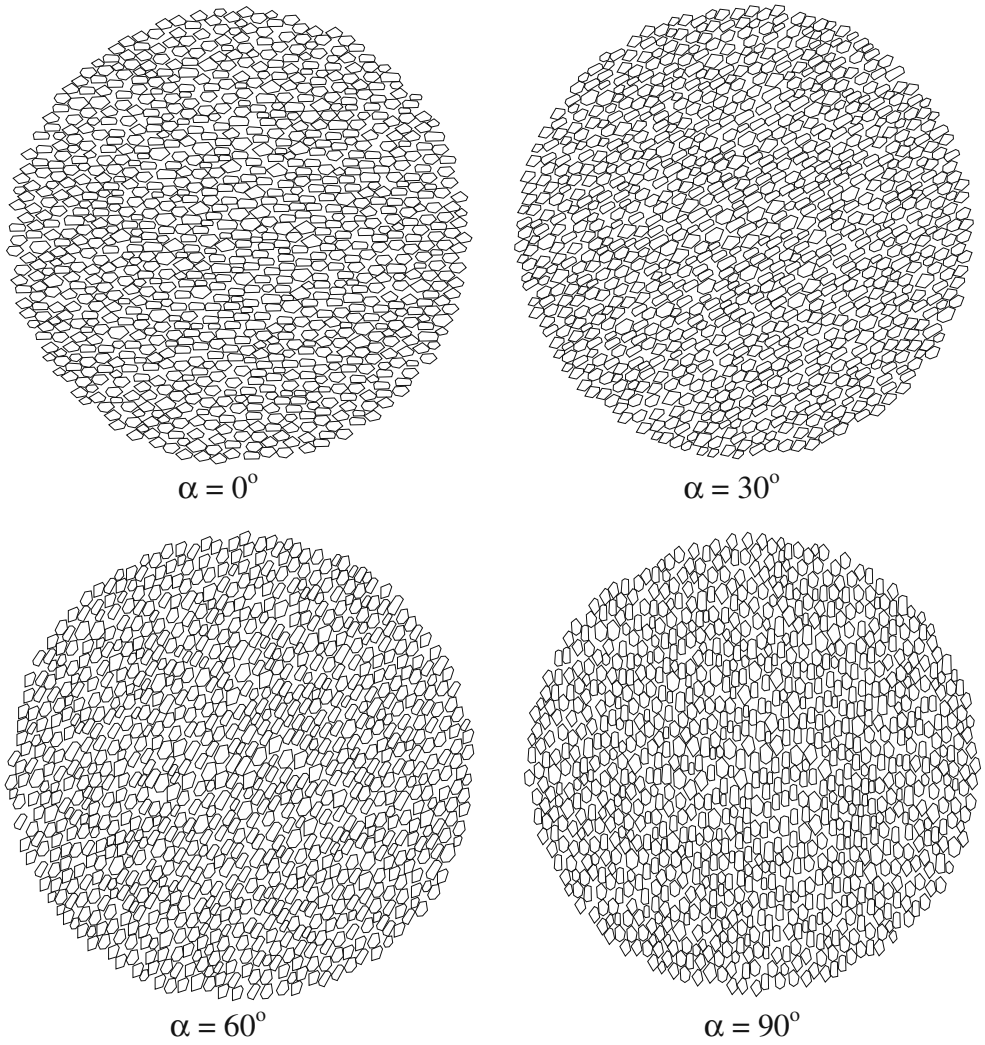

Fig. 5 Schemes of initially-generated numerical specimens with different bedding planes (α)

compaction is required. This compaction is performed by radial movement of boundary particles towards the center of the specimen. During this stage of simulation, the inter-particle coefficient (μ_s) is intentionally set to zero in order to facilitate the compaction process. In addition, the rotational damping of particles is assigned to a high value to restrict the rotation of particles. The compaction continues until a small amount of stress is mobilized inside the specimen, which means that particles are in contact with each other. Hereafter, the specimens are ready for being tested under applied loads.

3.3 Loading of specimens

Similar to what is performed in conventional laboratory tests on soil samples, each numerical simulation test consists of primary compression of the specimen under constant confining pressure followed by applying a deviatoric stress on the assembly. All specimens are firstly compressed isotropically under a confining pressure of 300 kPa. During the compression process, the isotropic loading continues until there is no volume change along with numerical cycles. The value of void ratio at the end of the isotropic compression process is 0.252, 0.259, 0.260, and 0.253 for the specimens with $\alpha = 0°, 30°, 60°,$ and 90°, respectively. The isotropically compacted sample with $\alpha = 30°$ is shown in Fig. 6a for an example. As the second stage of loading, the specimen is loaded biaxially in such a way that the stress in the lateral direction (1-1) remains constant and equals $\sigma_{11} = 300$ kPa, while the top and bottom of the specimen is loaded vertically along 2-2 axis by moving boundary particles with a constant displacement rate proportional to the distance from the center of the specimen. Accordingly, the specimen deforms under such biaxial loading condition and the circular form turns into an elliptical one, which is elongated horizontally (Fig. 6b).

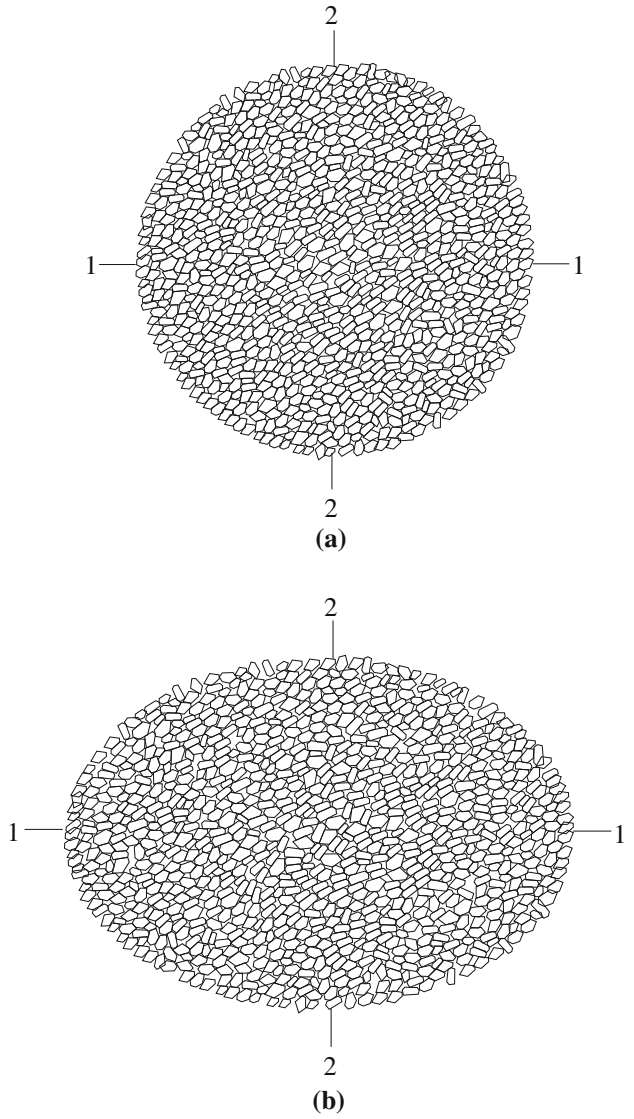

Fig. 6 Presentation of numerical specimens under **a** confining pressure of 300 kPa, **b** biaxial compression test (at axial strain of 16 %)

The values of DEM parameters used in the simulations are shown in Table 1. During loading stages, the inter-particle coefficient is set to $\mu_s = 0.5$. This value corresponds to the friction angle of quartz sand measured in laboratory [50]. The value of other parameters is chosen tentatively based on experiment and empirical trials so that reasonable results can be derived from simulations. The values of parameters are also well consistent with those reported in DEM-based researches in the literature [48,51]. It is important to point out that the behavior of 2-D numerical particles might be different from those of real 3-D sand particles. For instance, void ratio values obtained in 2-D simulations are much smaller than those in 3-D simulations. However, the mechanisms obtained in either real tests or 2-D simulated tests have been found to be analogous. As a consequence, the application of 2-D DEM analyses can help us to investigate the behavior of such discrete assembles more qualitatively rather than quantitatively.

Table 1 DEM parameters used in simulations

Parameter	Value
Vertical axial strain rate	0.003
Time step increment (Δt)	1.2×10^{-5} s
Particle density	2, 500 kg/m^3
Inter-particle friction angle (φ_μ)	26.6°
Cohesion between particles (C)	0.0 kPa
Normal spring constant (k_n)	2.0×10^8 N/m
Tangential spring constant (k_s)	2.0×10^8 N/m
Viscous translational dumping coefficient (α_m)	10,000
Viscous rotational dumping coefficient (α_I)	10,000

4 Simulation results

The results obtained from the simulations can be investigated from two different aspects as macroscopic and microscopic points of view.

4.1 Macroscopic behavior

In soil mechanics, it is a common practice to study the soil behavior by means of shear strength and compressibility characteristics, which are mainly influenced by stress level and density. In granular soils, shear strength is usually known by the so-called internal friction angle (ϕ) which is mobilized during shear deformation. By referring to the applied stress tensor on the specimens and using the conventional Mohr-Coulomb failure criterion, the mobilized internal friction angle (ϕ_{mob}) can be obtained:

$$Sin\phi_{mob} = \frac{\sigma_{22} - \sigma_{11}}{\sigma_{22} + \sigma_{11}} \tag{8}$$

where σ_{11} and σ_{22} are minor (in the horizontal direction) and major (in the vertical direction) principal stresses, respectively. $Sin\phi_{mob}$ can be interpreted as stress ratio too. Figure 7a presents the variation of mobilized shear strength of all numerical specimens in terms of $Sin\phi_{mob}$ against the axial strain (vertical strain in the tests). As shown, although the initial condition of all samples regarding the confining pressure and void ratio is the same, they show different manners in stress ratio variation. It is obvious that this difference in behavior arises from the initial fabric condition. According to this graph, the stress ratio increases rapidly until a small axial strain of 2 % and thereafter, the response differs. In the sample with $\alpha = 0°$, $Sin\phi_{mob}$ continues to grow and reaches a peak value in the axial strain of 7 %, while this

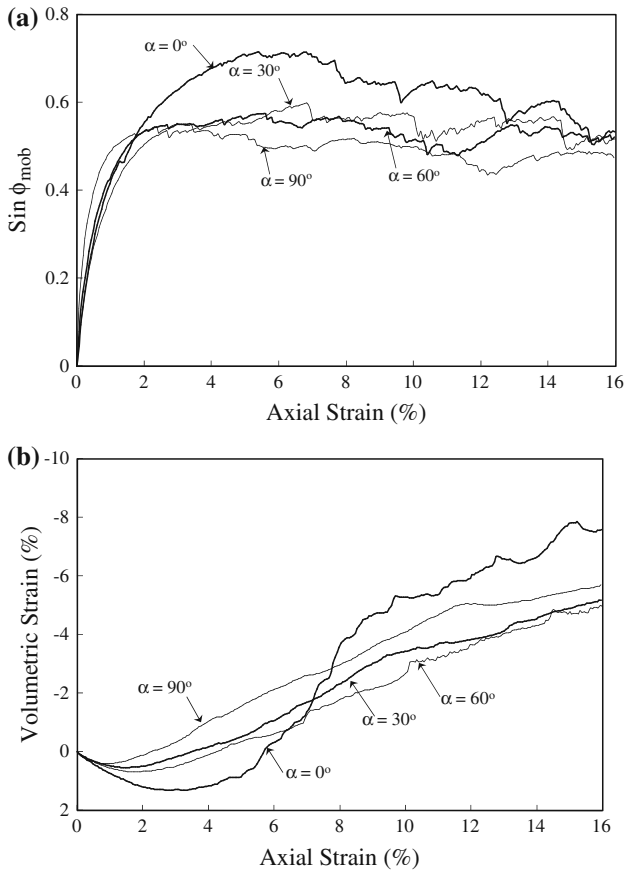

Fig. 7 Variation of **a** shear strength and **b** volumetric strain against axial strain for samples with different bedding planes (α)

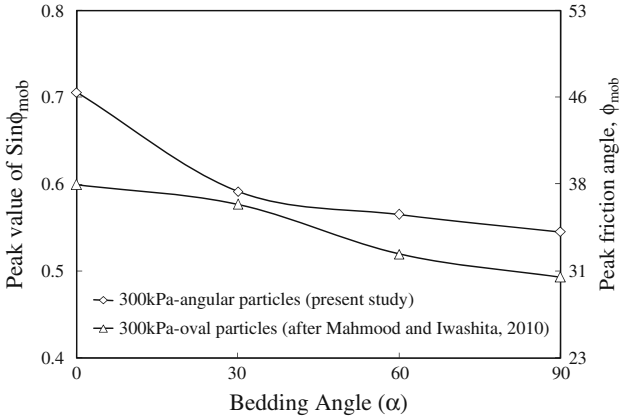

Fig. 8 Relationship between peak shear strength and bedding angle for samples with oval and angular particles

growth in other samples is much lower; $Sin\phi_{mob}$ continues to increase gradually with some fluctuations in the samples with $\alpha = 30°$ and 60°, but the growth has stopped in the sample $\alpha = 90°$ and instead, the shear strength falls along with the axial strain.

Regarding the effect of inherent anisotropy on deformational characteristics, the variation of volumetric strain versus axial strain is plotted in Fig. 7b. All samples behave contractively first, but they start to dilate afterwards. Although the dilative behavior of all samples initiates just before the mobilized shear strength reaches the peak value, the samples reflect different dilative behaviors. For example, the most initial densification occurs for $\alpha = 0°$ and the volume expansion initiates at about $\varepsilon_{22} = 3\,\%$, while the other samples start to dilate at very small axial strain level. By following the variation of the volume change, on the other hand, it can be found out that among the dilative behavior of samples, the sample with $\alpha = 0°$ has the greatest degree of dilation. This tendency in the deformational behavior has been observed too in numerical simulations performed by Mahmood and Iwashita [48] and Sazzad and Suzuki [51].

The variation of the peak value of $Sin\phi_{mob}$ with respect to the change of bedding angle is summarized in Fig. 8. As can be seen, the peak stress state is obtained maximum for $\alpha = 0°$ and it decreases as the bedding angle increases. In the same figure, the result of another series of DEM-based simulations is presented [48,51]. In this series, several plane strain tests were simulated under lateral pressure of 300 kPa. The particles were elliptical with the aspect ratio and particle size similar to this paper. According to Fig. 8, both series of simulations have the same trend in the variation of maximum value of $Sin\phi_{mob}$. Nevertheless, the values corresponding to the tests in this paper are obtained higher than those with elliptical particles. The difference in results can be explained by considering the effect of interlocking phenomenon among angular particles. According to Lambe and Whitman [42], the value of the mobilized friction angle can be interpreted as the inter-particle friction angle plus the degree of interlocking whose value depends on the particle size and shape. Therefore, it is expected that a higher friction angle be obtained for angular particles in comparison with rounded particles. The effectiveness of particle shape on the shear strength has been found by many researches either in experimental [52,53] or numerical simulated tests [47,54,55].

4.2 Microscopic behavior

The macroscopic mechanical behavior of a granular material is intrinsically dependent on the evolution of microstructures during shear deformation. The observed variations in the mobilized shear strength and dilatancy can be well interpreted as a reflection of fabric evolution during loading. In the following sections, it is aimed to study different behaviors observed in inherently anisotropic samples from micromechanical point of view.

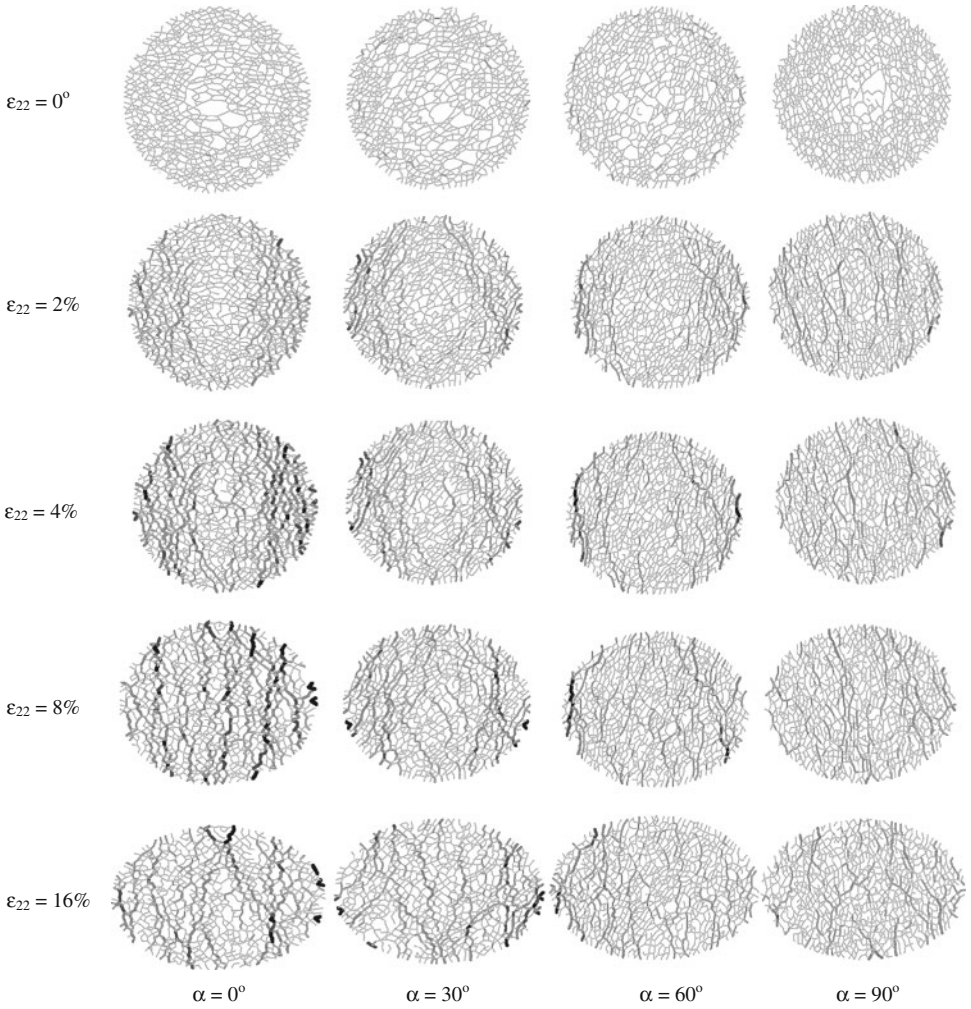

Fig. 9 Contact normals distribution at different axial strains with different bedding planes

4.2.1 Observational investigations

The significance of anisotropy in granular materials originates generally from preferred contact normals, preferred alignment of particles, and their associated voids. By studying fabric evolution during plane strain tests [21] on sands and biaxial compression tests on rod particles [17,56], dramatic changes in the number of contacts, particle inclination, and generation of large voids were figured out.

Contacts between particles play the leading role in the global behavior of granular materials since applied forces are supported by means of these connections. Figure 9 presents a graphical distribution of contact normals generated among the particles at different axial strain levels during the biaxial compression tests. Contact normals indicate the normal direction of contact planes between two particles. They are depicted as straight lines with different colors and thicknesses, which represent the magnitude of forces normalized by the maximum value obtained in all tests. The lines become darker and thicker as the magnitude of the contact force increases. Before the biaxial compression test starts i.e., $\varepsilon_{22} = 0$, the contact normals are distributed directionally in each sample although the samples have been loaded under an isotropic condition. It is found out that the majority of contact normals are oriented along the bedding angle. This is more recognizable in the internal parts of the samples. In addition, there is a uniformity found among the contacts concerning the magnitude. From a micromechanical standpoint, such spatial distribution in contacts signifies the concept of 'inherent anisotropy' in granular materials. By applying deviatoric stress along 2-2 axis, the initial order in contacts alters gradually during shear deformation. By comparing the distribution of contact normals, it is seen that new contacts are generated along the bedding plane of particles. Furthermore, the existing contact forces become greater in such a way that continuous chains of contact normals are formed tending to be aligned in vertical direction along major principal stress. Stronger contact chains are formed sooner at the lateral parts of the specimens close to the boundary, because they are shorter in length and thus, they can transfer the applied stress more efficiently in relation to long chains inside the samples. The evolution found in the contact distribution is referred to as 'induced anisotropy', which is the consequence of generation and/or disappearance of contacts. This evolution justifies

the variation of mobilized shear strength shown in Fig. 7a. For instance, by comparing the contact normal distribution at different strain levels in the sample $\alpha = 0°$, it is clear that it has the largest amount of strong contacts at $\varepsilon_{22} = 8\,\%$. This finding agrees well with the peak value of mobilized shear strength around this level of deformation. For other samples, this comparison might be visually difficult and such microscopic observations are studied later quantitatively in following sections.

The contact anisotropy either existed at the initial condition or induced during the loading process is owed to the particles arrangement within the samples. Figure 10 illustrates the position of particles related to each other at axial strain levels of $\varepsilon_{22} = 2, 4, 8,$ and $16\,\%$. In order to follow the particle arrangements within the assemblies and similar to the graphical method used for contacts, the particles are colored by different degrees of darkness depending on the amount of applied forces; the darker particles support bigger forces. In Fig. 10a, the particles loaded by less than average value are omitted, while Fig. 10b presents the arrangement of particles which are loaded higher than half of the maximum force value. From the onset of loading, it can be figured out that the particles tend to create microstructures in the form of columns along vertical direction in order to transmit the applied deviatoric stress. During loading, there are some columns that come into existence, collapse, are shortened, or even are regenerated. In the sample with $\alpha = 90°$, the development of such microstructures is generally scattered within the medium during loading, while the development pattern is different in other samples. It can be seen that the side particles are the first ones to accept applied stresses and then the development of column-like structures is distributed towards the center of the assemblies. The density (the number per volume) of such microstructures is found to be higher in the sample with $\alpha = 0°$ compared to other samples, which becomes the highest at about the axial strain of 6–8 %. According to the particle arrangement patterns seen in Fig. 10a, b, the column-like structures become shortened or disappear in assemblies with $\alpha = 60°$ and $90°$, which justifies the lower shear strength of assemblies. However, there is a high concentration of force chains in the assembly with $\alpha = 0°$. This phenomenon, in addition to the contact distribution already described in Fig. 9, can justify the peak shear strength observed in $\alpha = 0°$ at the above mentioned axial strain range.

By comparing the density of column-like structures in Fig. 10a with that in Fig. 10b, it can be seen that the number of particles partaken in the force chains is reduced if the particles with forces lower than half of the maximum value are neglected. This indicates that although the particles carrying above average load (Fig. 10a) appear to form a network of forces, the majority of particles belongs to a weak network and rather, stronger force chains are more shortened and scattered through the medium (Fig. 10b). The quantification of the density, length, and the distribution of such force chains needs to define a criterion in terms of factors such as the number of incorporated particles and the magnitude of carrying forces [57–59]. This subject is out of scope of this study and it can be considered as an open issue to be addressed in future works.

By focusing on the evolution of columns during loading process, as already explained in the Sect. 1, arrays of gaps can be found to be generated among microstructures. It can be recognized that although the size and location might differ, the distribution of such voids throughout the sample does not change abruptly during different loading stages (It is reminded that only high-stressed particles are considered here). There is an exception and that is for the sample $\alpha = 0°$. From the beginning of loading in this sample, the development of microstructures continues and the initial gaps are closed and replaced by new columns until the axial strain of 8 %. Hereafter, it seems that such progressive trend is switched off and in turn, the columns seem to buckle which result in large openings between them. Such happening can be figured out easily at the axial strain of 16 %. Paying attention to the macroscopic deformational behavior of the sample $\alpha = 0°$, as already discussed, one can consequently interpret the contractive behavior as well as the following dilation of the sample. The reduction in volume directly corresponds to the construction of columns and filling voids. However, the occurrence of column buckling motivates the dilative behavior. This explains why the dilative behavior of samples takes place after the peak stress state. It can be seen that the slope of the volumetric strain versus axial strain curve of this sample ($\alpha = 0°$) starts to augment at the axial strain of 8 % (Fig. 7b), which corresponds the start of the post peak stress state (Fig. 7a). This point of behavior coincides with the initiation of columns buckling and the generation of large voids. As mentioned before, these observations agree well with the findings on real sand tests in laboratory [20,21].

As a complementary standpoint about the microscopic inspections, it is focused on the stability of column-like microstructures within assemblies. As explained before in the Sect. 1, the formation of such column-like structures has been already proved by researchers. Here, it is tried to justify the observed difference in the distribution pattern of such structures within inherently-anisotropic granular materials and its relation to the mechanical behavior. The difference in response of assemblies arises from the local and global stability of such columns. The local stability relates to the alignment of a particle with respect to the loading direction. According to Fig. 11a, a particle with the horizontal long axis under a couple of forces (F) remains in a steady state against rotation, while for a similar particle with vertical alignment, there is a high tendency to rotate because of a torque (M) initiated from a small eccentricity of forces (d). As a

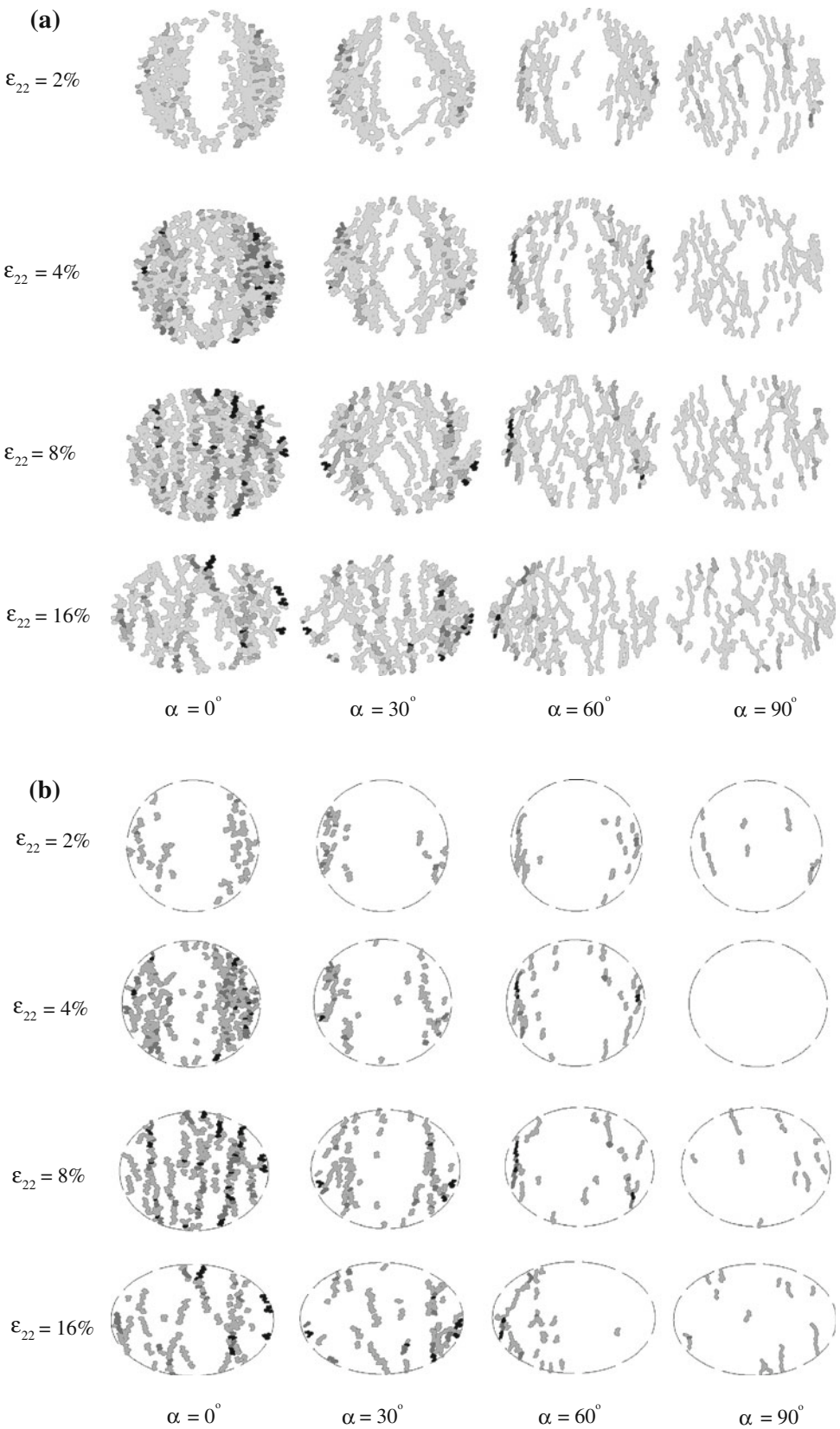

Fig. 10 Presentation of loaded particle arrangements inside the samples with different bedding planes. *Dark* particles are highly loaded and less-loaded particles are *light gray*. **a** Particles with forces lower than average value are omitted. **b** Particles with forces lower than half of maximum value are omitted

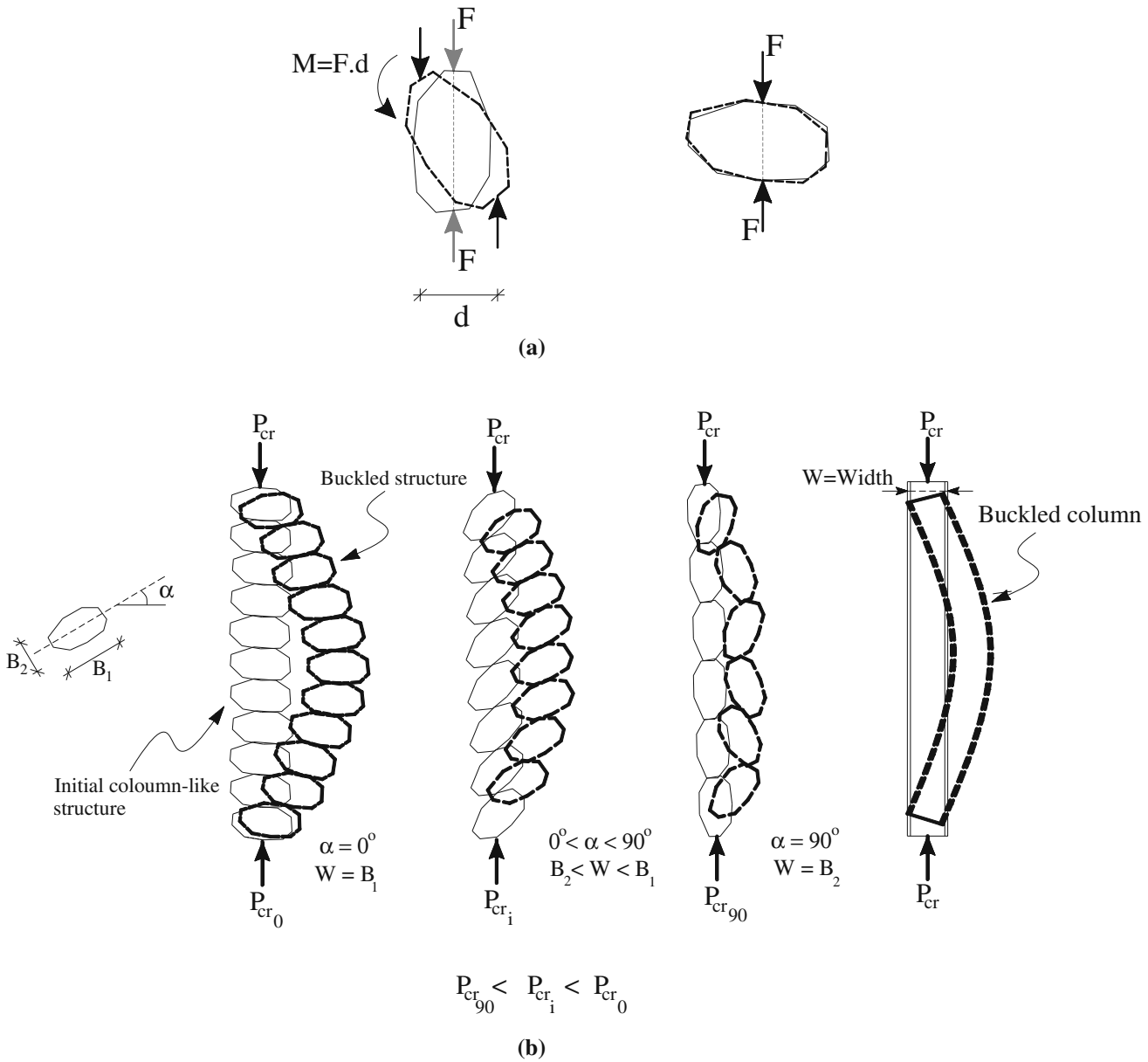

Fig. 11 **a** Stability of a *horizontal* and *vertical* particle under a couple of forces; **b** Schemes of a simple model for microstructures as a column and the relationship among critical loads (Pcr) and width of buckled columns

consequence, it can be found that the sample with $\alpha = 90°$ rarely contains continuous long columns. Regardless of such local instability, on the other hand, the geometry of generated granular columns plays an important role in the global stability of such structures. Consider three column-like structures with the same length L, according to Fig. 11b, which are constructed by stacking of similar particles with $B_1 \times B_2$ dimensions. The column-like structure, whose particles are horizontally oriented, has the largest width (B_1) while the structure slims as the particle bedding angle increases so that the column with vertical particles has the least width (B_2). As already known for a structural problem, the buckling load (P_{cr}) of a column increases with the width (W). Accordingly, the columns generated in the sample with $\alpha = 0°$ are more stable than those in other samples.

4.2.2 Fabric anisotropy

In the previous section, the evolutions happened in the fabric within the inherently-anisotropic assemblies were described graphically. Hereafter, it is aimed to study the fabric change from quantitative point of view.

As mentioned before, one of the factors causing the fabric to be anisotropic is the distribution of particle orientation.

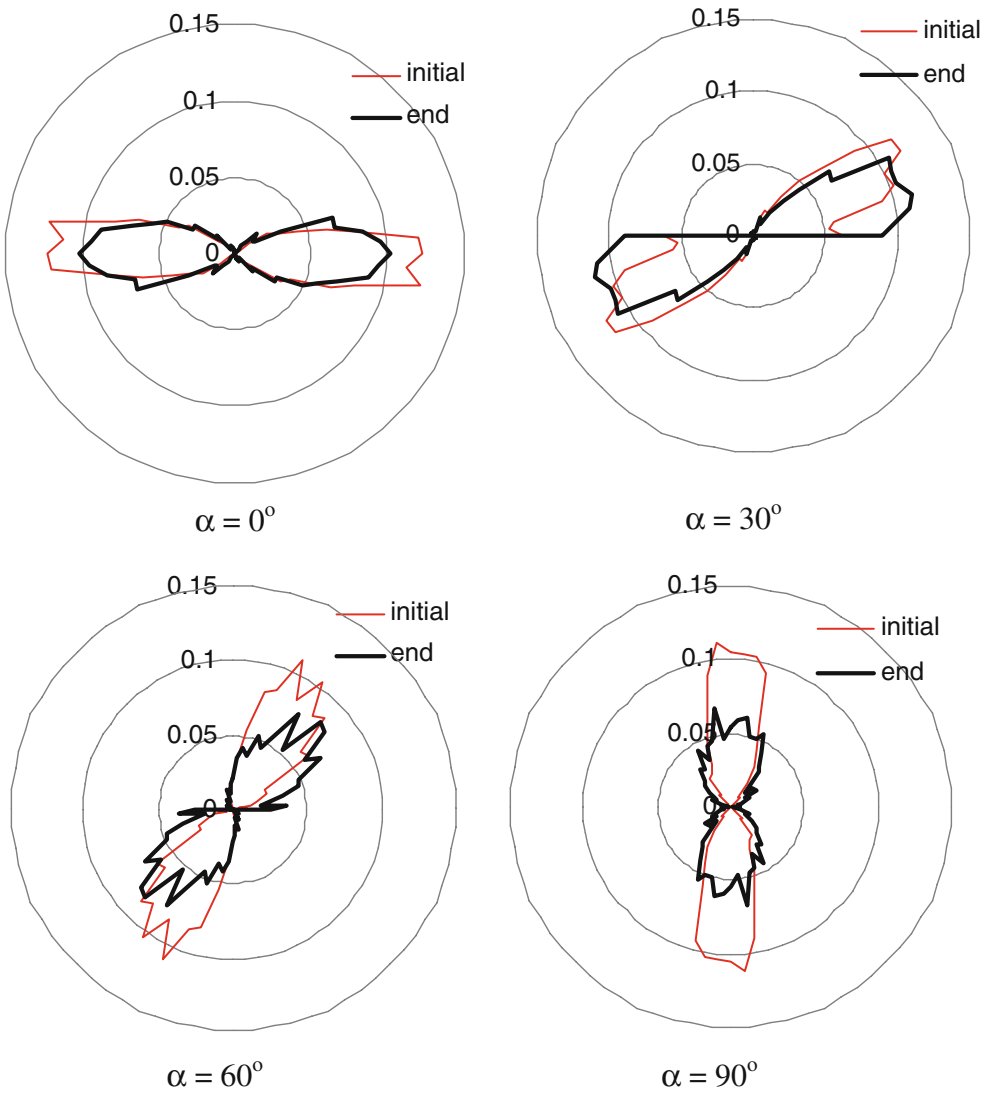

Fig. 12 Polar distribution of long axis of particles with respect to the horizontal within inherently-anisotropic assemblies

Figure 12 shows the angular distribution of particle orientation for initial condition and at the end of the biaxial test. The graphs present the portion of particles (the ratio of the number of particles to the total number of particles) with respect to the angle from the horizontal. A particle is considered in the numeration if its long axis is oriented within five-degree intervals. Generally, in a granular material, in which the particles are randomly positioned, there is an isotropic distribution of particle orientation through the sample and thus, the graph forms close to a circle. However, as seen in Fig. 12, such distribution in inherently-anisotropic assemblies has a wing-like form along the direction of bedding plane. Regardless of the direction of anisotropy, the initial distribution of all samples is analogous and the maximum portion is around 0.11. Nevertheless, such repartition during shear deformation changes in different manners depending on the initial bedding angle. Such induced change can be figured out by comparing the initial orientation distribution with that at the end of loading process. The direction of anisotropy is without change in the cases $\alpha = 0°$ and 90°, but the distributed number of particles has been altered. Such evolution has taken place more significantly for $\alpha = 90°$ as a 50 % reduction in the maximum portion. It is reminded that this alteration observed in the fabric corresponds to the rotation of particles which can be interpreted as a consequence of the buckling of columns already described in the previous section (also refer to Fig. 11a). In the sample $\alpha = 30°$, a reverse tendency is found, which indicates that the portion of particles compared to the initial condition remains almost constant, but the direction of anisotropy is rotated clockwise. Similarly, the evolutions observed in the sample $\alpha = 60°$ includes the clockwise rotation of the particle inclination anisotropy as well as the reduction in the number of particles in a specific direction.

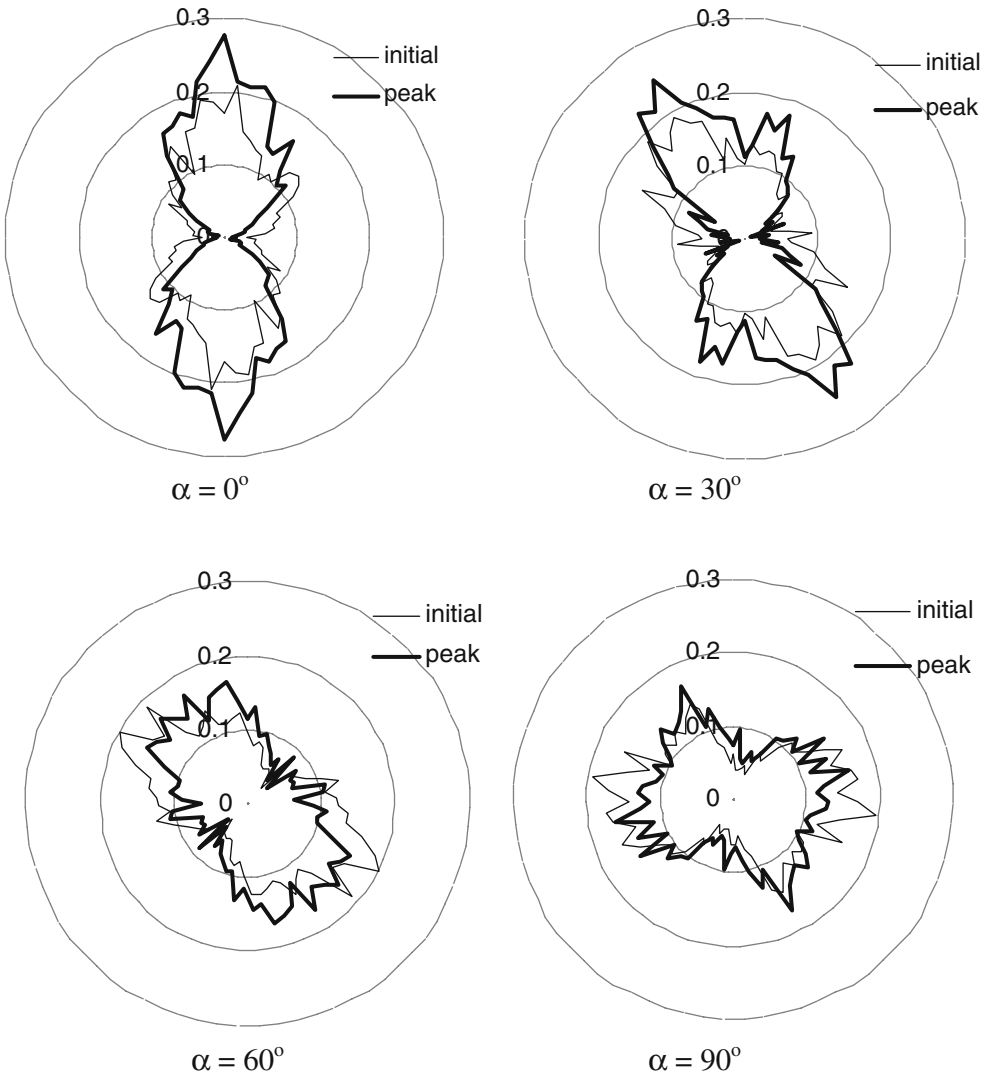

Fig. 13 Polar distribution of contact normals at initial state (*thin line*) and peak stress state (*thick line*) for different bedding angles (α)

The importance of contacts in a granular material originates from the fact that forces are carried by contact between particles. To show the arrangement of contacts, an angular distribution similar to that of particle orientation is used. The distribution of contact normal orientation is determined as the fraction of all assembly contact normals that falls within the orientation intervals of five degrees. Figure 13 shows the polar histograms of contact normals for initial and peak stress states of the tests for different bedding angles. It can be said that the normal contact anisotropy is highly dependent on the orientation of particles since the direction of contact normal anisotropy varies from one assembly to another assembly. Moreover, by comparing these two states, it seems that the histograms deform like being widened/shortened from initial to peak stress state.

In order to quantitatively follow the degree of contact normal anisotropy during the loading process, the change in the form of histograms can be studied by introducing major principal direction of fabric anisotropy (θ_c) and coefficient of contact normal anisotropy (a_c). The parameter θ_c indicates the angle between the long axis of the histogram with respect to the loading axis (vertical direction). The meaning of the parameter a_c becomes clear if it is noted that the number of contacts oriented along the major principal direction of anisotropy (θ_c) is proportional to $1 + a_c$ while the number of contacts oriented along the perpendicular direction is proportional to $1 - a_c$. In other words, the parameter a_c indicates the elongation of histograms and can be defined by $a_c = (A_1 - A_2)/(A_1 + A_2)$, in which A_1 is the length of the axis of the histogram along the major principal direction and A_2 is that along the perpendicular direction. The value of a_c varies from zero to one. If the histogram has the form of a circle, the a_c value is zero, which corresponds to an isotropic distribution. However, the value of a_c increases and closes to

one if the circle deforms as a peanut, which indicates a high degree of anisotropy condition.

By assuming that the data of a polar histogram for contact normals (like what presented in Fig. 13) be approximated by a second-order Fourier series, the parameters a_c and θ_c can be determined by using least square regression of histogram data as follows:

$$a_c = \sqrt{A_s^2 + A_c^2}$$
$$\theta_c = \frac{1}{2}\tan^{-1}\left(\frac{A_s}{A_c}\right) \quad (9)$$

In the above equations, $A_s = \frac{1}{N_c}\sum_{i=1}^{N_c} Sin2\theta_i$ and $A_c = \frac{1}{N_c}\sum_{i=1}^{N_c} Cos2\theta_i$, where θ_i indicates the orientation of ith contact normal from the loading axis (reminded that N_c is the number of total contacts). This procedure is described in greater details by Rothenburg [43] and Rothenburg and Bathurst [60].

The variation of contact normal anisotropy coefficient (a_c) and the major principal direction of fabric anisotropy (θ_c) versus axial strain for all samples are shown in Fig. 14. According to Fig. 14.a, the initial value of the anisotropy coefficient a_c is the same for all samples ($a_c = 0.5$). This means that all samples have the same degree of anisotropy and a unique distribution of contacts exists within all samples regardless of dissimilar bedding planes. This is expected since at the end of compaction, all samples have the same condition regarding the compaction state (or void ratio) as well as stress level (or confining pressure). However, the variation of the anisotropy coefficient (a_c) follows different manners during shear deformation. In the sample $\alpha = 0°$, the anisotropy coefficient increases with axial strain up to the peak value of around one and then it falls a little and remains constant up to the end of the test. The increasing trend in the anisotropy coefficient suggests the phenomenon in which, new contacts are generated along the anisotropy direction (perpendicular to the bedding plane) and disintegration of contacts in the lateral direction. Similarly, the parameter a_c in the sample with $\alpha = 30°$ increases monotonically from the onset of loading and it reaches a constant value at large axial strain of 10 %, but smaller than that in the sample $\alpha = 0°$. The least change in the fabric anisotropy belongs to the sample with $\alpha = 60°$ since the coefficient a_c stays almost constant at around 0.5 duringthe shear deformation. Finally, for the sample $\alpha = 90°$, it can be seen that the contact normal anisotropy coefficient always has a decreasing trend which gradually closes to zero at larger axial strains. As explained before, the growth in a_c, like what happens in the samples with $\alpha = 0°$ and 30°, indicates that the number of contacts along a direction intensifies with respect to other directions. Reversely, the reduction of a_c for the sample $\alpha = 90°$ implies that the contacts between

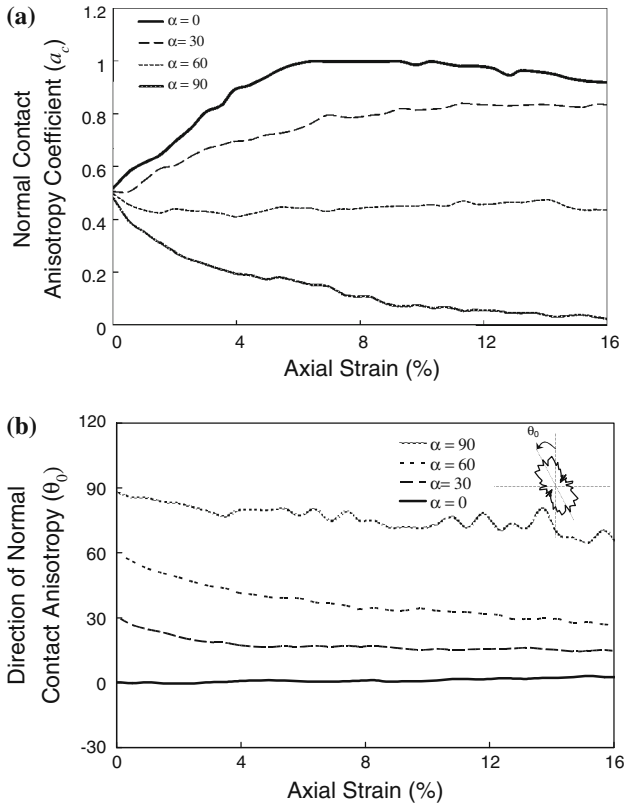

Fig. 14 Variation of anisotropy parameters along with axial strain within all bedding angles: **a** normal contact anisotropy coefficient; **b** direction of normal contact anisotropy

particles have the tendency to be distributed isotropically within the assembly. The variation of rotation of anisotropy direction is presented in Fig. 14b. As can be seen, the initial value of θ_c coincides with the initial bedding angle for all assemblies. However, different trends can be observed in the orientation of principal direction of fabric anisotropy during loading process. The anisotropy principal direction (θ_c) does not change significantly in $\alpha = 0°$, while it has a decreasing trend in other cases. In the assembly with $\alpha = 30°$, it falls rapidly to 15° at small axial strain of about 5 % and it becomes constant up to the end of the test. In the assembly with $\alpha = 60°$, the reduction in θ_c continues to the end of the test, which implies the most change in the direction of anisotropy among other samples. In this sample, the principal direction of anisotropy rotates 30° towards the loading axis. Paying attention to the fact that the anisotropy coefficient in this sample remains constant, but the anisotropy direction rotates towards the loading axis, suggests that the number of new forming contacts along the loading direction is the same as the number of disintegrated contacts in the lateral direction and these two phenomena happen concurrently. The direction of anisotropy in the assembly with $\alpha = 90°$ has a total reduction of 20° from the start point accompanying with some fluctuations, which indicates the instability

of particles arrangements discussed before. The same trend in the variation of the contact normal anisotropy parameters is observed in numerical simulations with elliptical particles performed by Mahmood and Iwashita [48].

4.2.3 Force anisotropy

In the previous section, only the number of contacts in a polar distribution is considered as fabric anisotropy. In a similar way, the magnitude of contact forces with respect to the contact orientation is investigated in terms of normal and tangential force components. To do so, the magnitude of contact forces including normal (f_n) and tangential (f_t) components are determined for each contact and the average value within angular intervals $\Delta\theta$ is calculated. The polar distribution of average normal contact force $\bar{f}_n(\theta)$ and average tangential contact force $\bar{f}_t(\theta)$ are calculated as follows:

$$\bar{f}_n(\theta) = \frac{1}{N_c(\theta)} \sum_{i=1}^{N_c(\theta)} f_n^i, \quad \bar{f}_t(\theta) = \frac{1}{N_c(\theta)} \sum_{i=1}^{N_c(\theta)} f_t^i \tag{10}$$

In the above equations, $N_c(\theta)$ is the number of contact normals whose direction belongs to the range of $\theta \in [\theta - \Delta\theta/2, \theta + \Delta\theta/2]$. By plotting the average contact forces in polar coordinates, the angular distribution can be obtained. In order to compare the magnitudes in different states of loading, the value of average (normal and tangential) contact forces is normalized by the global average normal contact force ($\bar{f}_0$) throughout the sample:

$$\bar{f}_0 = \frac{1}{2\pi} \sum_{i=1}^{N_g} \bar{f}_n(\theta_i)\Delta\theta \tag{11}$$

where N_g indicates the number of angular intervals. Figure 15 shows the plots of polar distribution of normalized average normal contact force ($\bar{f}_n(\theta)/\bar{f}_0$) at initial and peak stress states for all assemblies by considering angular intervals ($\Delta\theta$) of five degrees. The histogram of all samples at the initial state seems to have approximately a circular form, which indicates that the magnitude of average normal contact force is almost the same in all directions. This is expected since all samples were initially compacted under isotropic condition. The histograms, however, are elongated, at the peak stress state, along the loading axis and slimed along the horizontal direction. In addition, the long axis of all histograms is oriented along the loading axis, regardless of the bedding angle. This evolution in the normal force anisotropy suggests the development of new contacts as well as the increase in the magnitude of normal forces along the loading axis in relation to those in the horizontal direction.

In order to trace the variation of normal contact force anisotropy during shear deformation, a coefficient of normal contact force anisotropy (a_n) as well as major principal direction of normal force anisotropy (θ_n), similar to what is done for contact orientation, are defined based on the histogram data. By considering a second-order Fourier expression for polar distribution of average normal contact force component, the related anisotropy parameters a_n and θ_n can be calculated by using least square regression of histogram data:

$$a_n = \sqrt{F_s^2 + F_c^2}$$
$$\theta_n = \frac{1}{2}\tan^{-1}\left(\frac{F_s}{F_c}\right) \tag{12}$$

where $F_s = \frac{1}{\bar{f}_0}\sum_{i=1}^{N_g} \bar{f}_n(\theta_i) Sin2\theta_i$ and $F_c = \frac{1}{\bar{f}_0}\sum_{i=1}^{N_g} \bar{f}_n(\theta_i) \cos 2\theta_i$. Figure 16 presents the variation of the parameters a_n and θ_n for all samples against the axial strain. According to Fig. 16a, the initial value of the normal force anisotropy coefficient (a_n) is not zero for any samples, but has a very small value, which arises from the bedding angle of particles. In the sample $\alpha = 0°$, the parameter a_n increases gradually and reaches a peak value and then it falls accompanying by some fluctuations. On the contrary, the anisotropy coefficient in other samples rises quickly and reaches a peak value. Afterwards, although it slightly varies up and down as the axial strain increases, the general value remains constant till the end of the test. As a general view, the value of a_n has greater value as the bedding angle decreases. In fact, the rise and fall observed in the a_n value during the loading process correspond respectively to the generation and collapse of microstructures described before. For instance, by paying attention to the first fall in the sample with $\alpha = 0°$, it implies that the reduction in a_n coincides with the reduction observed in the shear strength as well as the high degree of dilation. As already explained, this point corresponds to the bulking of column-like structures. However, along with the loading process and by rearrangement of particles, new columns are generated and therefore, the parameter a_n increases again. The same phenomena happens in other assemblies but the rate of generation/disintegration of force chains is smaller in comparison with $\alpha = 0°$ and thus, smaller rise and fall can be seen in the variation of a_n. By looking at Fig. 16b, it can be seen that the direction of normal force anisotropy has abruptly rotated towards the loading axis i.e., $\theta_n = 0$, as soon as the loading process begins. The initial direction of normal force anisotropy coincides with the direction perpendicular to the bedding angle, though.

The same strategy is applied in studying the tangential component of contact forces within the samples. Figure 17 depicts the polar distribution of the average tangential contact force normalized by the global average normal contact force ($\bar{f}_t(\theta)/\bar{f}_0$) for all samples for the peak stress state. The initial tangential contact force inside the samples is close to zero, because the initial loading relates to an isotropic compaction and no shear deformation occurs. As a conse-

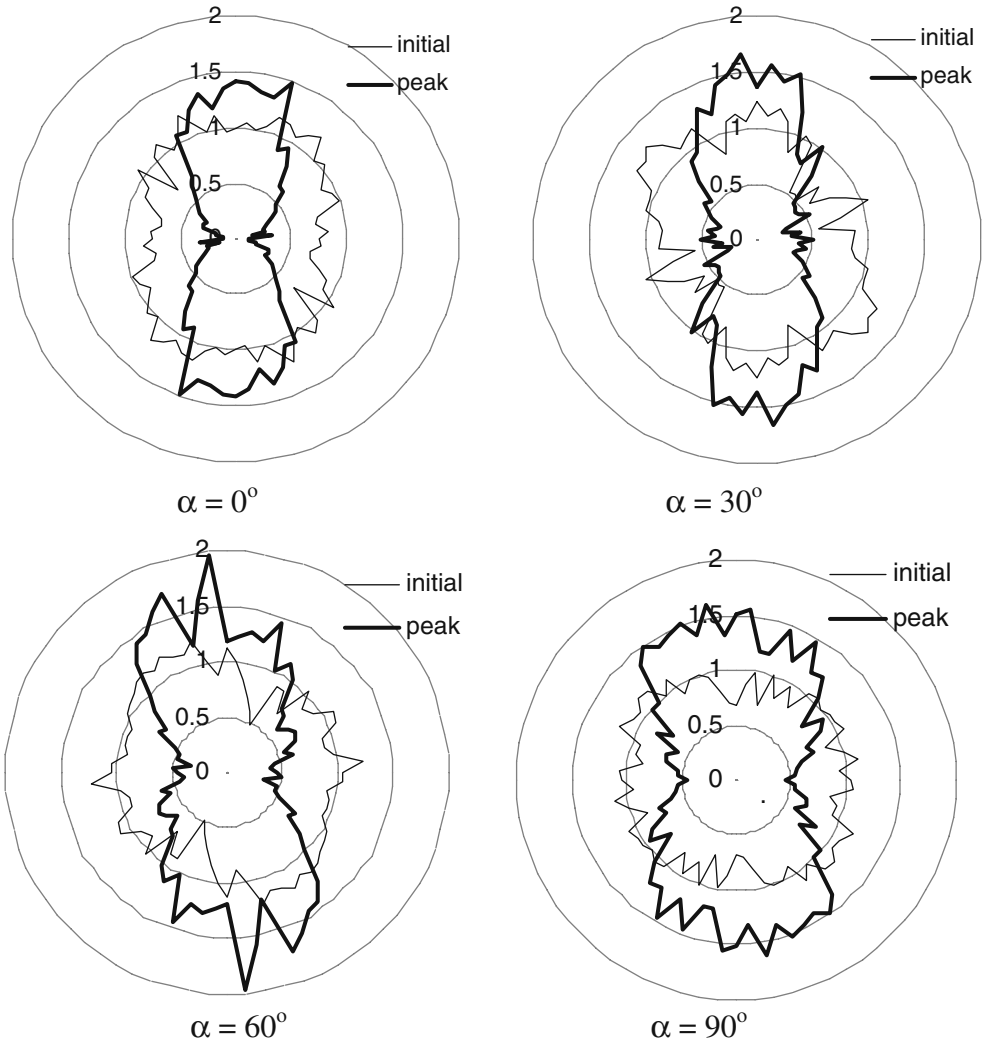

Fig. 15 Distribution of the normalized average normal contact force ($\overline{f}_n(\theta)/\overline{f}_0$) at initial (*thin line*) and peak stress state (*thick line*) for different bedding angles

quence, no shear stress is mobilized among particles. For the peak stress state, however, it can be found out that the polar distribution of tangential force is paraded by four leaps instead of having a peanut-like form such as happened for normal contact force distribution. The reason is clear if it is reminded that the direction of the tangential contact force is perpendicular to the normal contact force and thus, the distribution of tangential contact force differs. The inclinations of these leaps show the directions along which, high shear forces are concentrated. Furthermore, it can be seen that the polar distribution of contact tangential force is symmetric in $\alpha = 0°$ and 90°, but it has a nonsymmetrical form in the samples with $\alpha = 30°$ and 60°. This is due to the fact that the orientation of particles within the assemblies (i.e., bedding plane) influences the direction of the planes pertaining to maximum mobilized shear stress. Within the samples with $\alpha = 0°$ and 90°, where the particles alignment is symmetrical with respect to the loading axis, the shear planes are to be distributed symmetrically, while the non-symmetrical pattern of particles inclination in assemblies $\alpha = 30°$ and 60° causes to disturb the balance among shear planes generated among particles.

To follow quantitatively the changes of the anisotropy in tangential contact force distribution, the same procedure used for the normal contact force distribution is taken into consideration. By assuming that the polar distribution of average tangential contact force be approximated by a second-order Fourier expression, the coefficient of tangential contact force anisotropy (a_t) and the relating principal direction of anisotropy (θ_t) can be defined as:

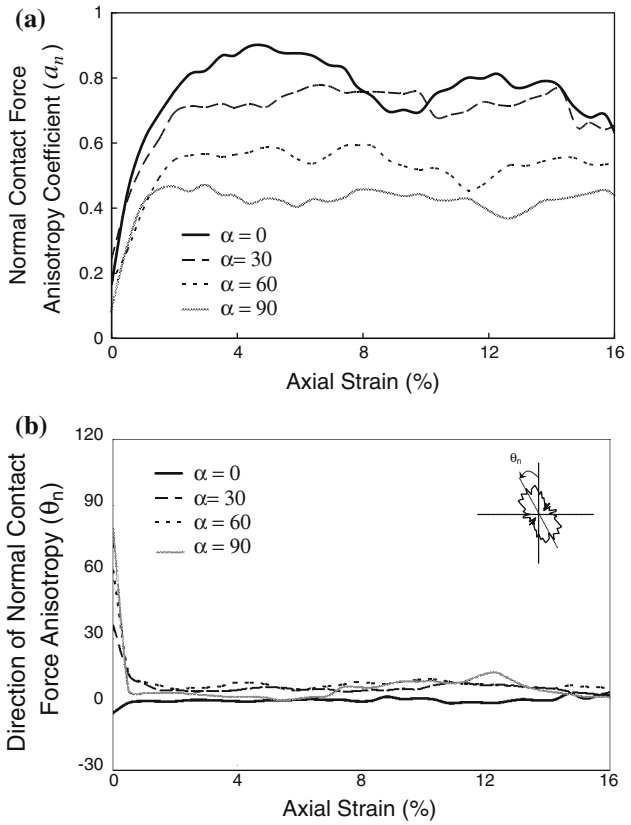

Fig. 16 Variation of normal contact force anisotropy parameters along with axial strain within all bedding angles: **a** normal contact force anisotropy coefficient; **b** direction of normal force anisotropy

$$a_t = \sqrt{T_s^2 + T_c^2}$$
$$\theta_t = \frac{1}{2}\tan^{-1}\left(\frac{T_s}{T_c}\right) \tag{13}$$

where $T_s = \frac{1}{\bar{f}_0}\sum_{i=1}^{N_g} \bar{f}_t(\theta_i) Sin2\theta_i$ and $T_c = \frac{1}{\bar{f}_0}\sum_{i=1}^{N_g} \bar{f}_t(\theta_i)\cos 2\theta_i$. Figure 18 presents the variation of the parameters a_t and θ_t versus the axial strain. As shown in Fig. 18a, there is a similar trend in the variation of a_t coefficient for all samples. It reaches a peak value at a small axial strain and then it slightly decreases towards the end of the test. The variation of a_t in $\alpha = 0°$ is a little different, where a_t is fully mobilized at larger axial strain and the following reduction becomes more compared to other samples. No relation can be detected between the peak value of a_t coefficient and the bedding angles. The variation of the corresponding principal direction of anisotropy (θ_t) is plotted in Fig. 18b. It explains that the rotation of tangential force anisotropy direction takes place at the beginning of the loading process. The principal direction of tangential force anisotropy (θ_t) rapidly orients along loading axis ($\theta_t = 0$) for the cases $\alpha = 0°$ and 90°, while it is inclined 10 degrees clockwise with respect to the loading axis in other samples ($\alpha = 30°, 60°$). As a consequence, by comparing the variation of θ_t with that of θ_n (Fig. 16b), it is concluded that the principal directions of normal and tangential contact forces are not coincident for $\alpha = 30$ and 60°. It is reminded again that this non-coincidence is because of the non-symmetrical pattern of particles orientation with respect to the loading axis within these two assemblies.

5 Conclusions

Naturally deposited soils show anisotropy in their mechanical behavior, which is a consequence of particle alignment along the bedding plane, contacts and associated voids between particles. Such initial condition signifies an inherent anisotropy in the fabric of granular materials. As a macroscopic point of view, the inherent anisotropy influences mechanical characteristics of soils including shear strength and deformability. It is obvious that the difference found in the mechanical behavior arises from microscopic evolutions in the fabric of granular media. Consequently, an investigation on the fabric change during the loading process is necessary for a better understanding of mechanical behavior. Another sort of anisotropy induced in the granular medium can be found during the shear deformation which justifies different trends observed in the mechanical behavior of granular assemblies.

In the present paper, a series of biaxial compression tests were carried out by applying the numerical DEM. The simulations consisted of four inherently-anisotropic assemblies with bedding angles of $\alpha = 0°, 30°, 60°$, and 90°. In these simulations, mechanical behavior of assemblies was studied from both macro and micromechanical points of view. By keeping in mind that sand grains are angular in shape, the main characteristic of this study was to consider the particles geometry as arbitrary convex polygons, while there are other simulations of granular assemblies in this filed with elliptical/oval particles. The main conclusions are summarized below:

(1) As already observed in experiment, the bedding plane of particles inside granular materials influences both shear strength and deformability. The peak shear strength of assemblies decreases as the bedding angle increases. In addition, the shear strength of angular particles is higher than that of rounded particles, which signifies the effect of particle shape and interlocking phenomenon among particles. The dependency of dilative behavior with regard to the bedding angle follows the same tendency.

(2) From a micromechanical standpoint, the peak value in shear strength relates to the existence of strong force chains within the samples. During the loading process, not only the number of contacts increases along the

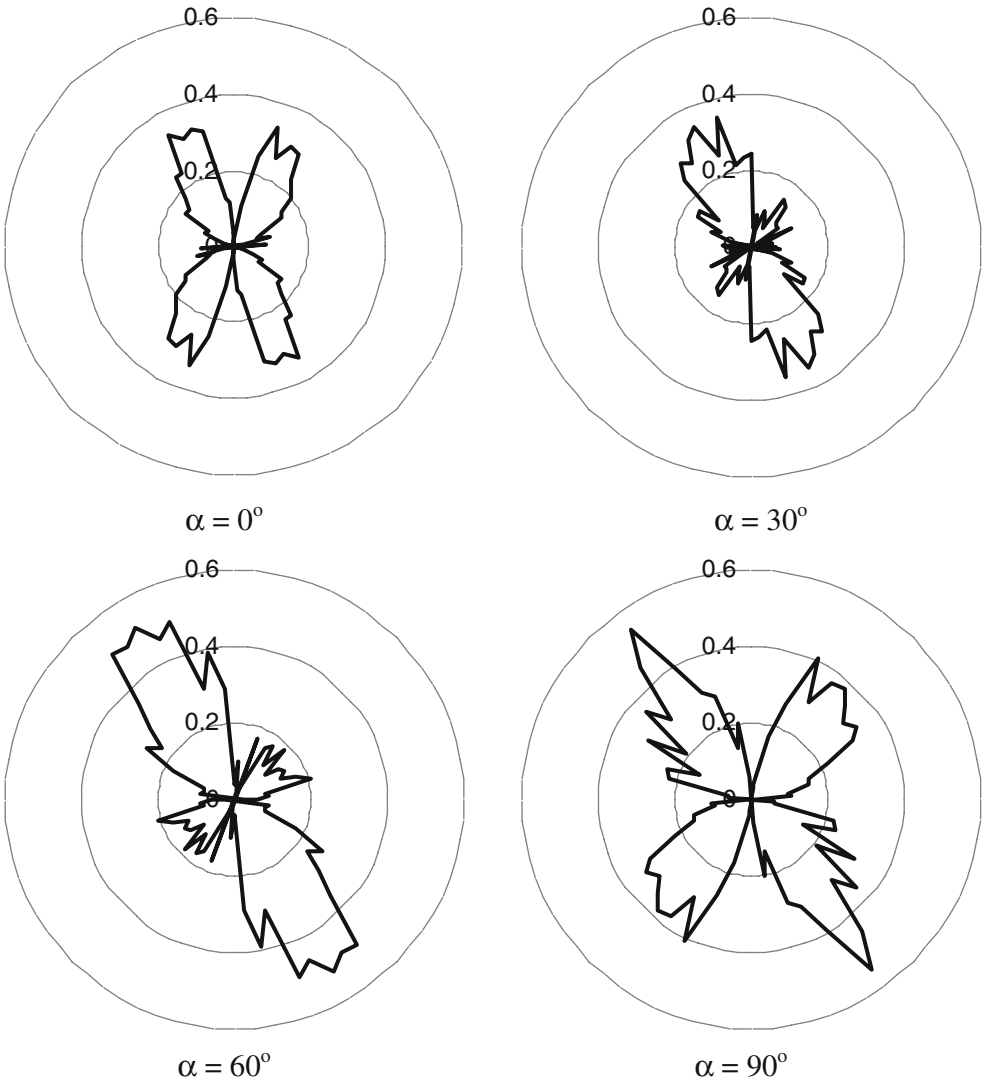

Fig. 17 Distribution of normalized average tangential contact force ($\overline{f}_s(\theta)/\overline{f}_0$) at peak stress state for different bedding angles (α)

loading axis, but also the magnitude of normal contact forces augments. This is verified by comparing the polar distributions of contacts and force contacts whose shapes tend to be elongated in direction of the loading axis.

(3) Based on simulations, applied loads on the granular materials are transmitted via column-like structures generated along the loading axis. As a consequence, the global behavior of assemblies is a function of the behavior of such force chains. The generation/disintegration of force chains justifies the increase/reduction of stress state in the assemblies. Moreover, the macroscopic dilative behavior of granular assemblies under shear does not only result from the buckling of force chains but also from the breakage of the interlocking between particles. This explains why dilative behavior takes place after the peak stress state.

(4) It is found out that the initial distribution of elongated particles and associated voids varies during shear deformation. The particles tend to be inclined in such a way that the long axis be oriented perpendicular to the loading axis.

(5) There is a tremendous difference in the development of the number of contact normals within inherently-anisotropic samples. According to the initial bedding angle of particles, contact anisotropy may be intensified (in $\alpha = 0, 30°$), remains unchanged (in $\alpha = 60°$), or the contacts tend to be distributed isotropically in the medium ($\alpha = 90°$) during shear deformation. In other words, the degree of anisotropy in the normal contacts amplifies with the deviation of the loading axis from the bedding plane of particles. However, the evolution of normal/tangential contact force anisotropy follows almost the same trend during the loading process.

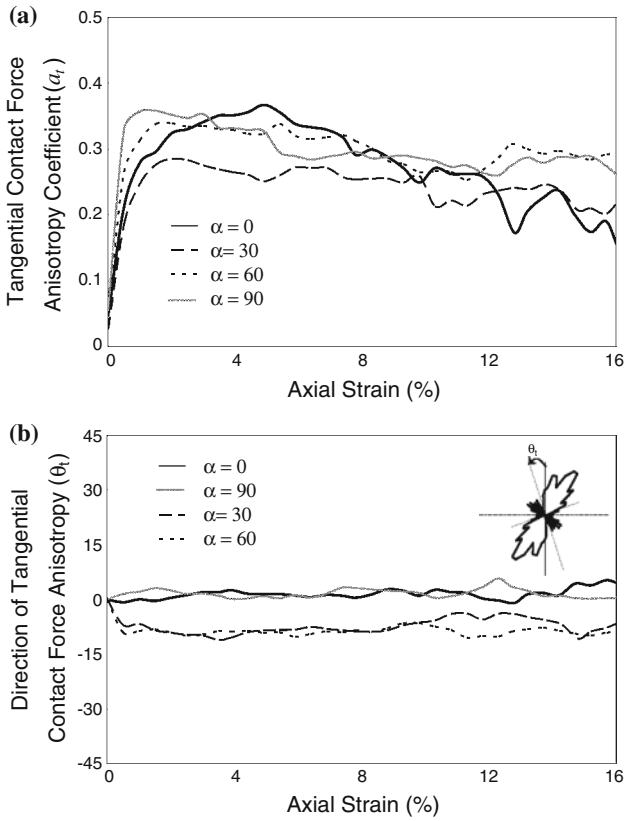

Fig. 18 Variation of tangential contact force anisotropy parameters along with axial strain within all bedding angles: **a** tangential contact force anisotropy coefficient; **b** direction of tangential force anisotropy

Normal contact force anisotropy is always mobilized to a peak value and then it tends to become constant accompanying by some fluctuations, while the tangential contact force anisotropy gradually decreases to the end of the loading process after reaching the peak value.

(6) The principal direction of normal contact anisotropy rotates gradually towards the loading axis along with shear deformation. Among all, the assembly in which the loading axis is perpendicular to the average bedding plane ($\alpha = 0°$), has the least change, while the assembly with $\alpha = 60°$ indicated the most rotation in the direction of normal contact anisotropy. On the other hand, the direction of normal/tangential force anisotropy abruptly changes and is inclined along the loading axis in all assemblies. This sudden rotation implies the rapid mobilization of stresses among particles. Furthermore, in contrast to the normal contact force, the distribution of tangential (shear) contact force is not symmetric within the assemblies where the bedding plane is neither parallel nor perpendicular to the loading axis.

Acknowledgments The author wishes to express his appreciations to Research Deputy of Ferdowsi University of Mashhad for supporting this project by grant No.: 18159-07/4/90. In addition, the author would like to express his gratitude to Dr. Ali Lashkari from Shiraz University of Technology in order to study the manuscript and give valuable comments.

References

1. Luding, S.: Anisotropy in cohesive, frictional granular media. J. Phys. Condens. Matter **17**, S2623–S2640 (2005)
2. Alonso-Marroquin, F., Luding, S., Herrmann, H.J., Vardoulakis, I.: Role of anisotropy in the elastoplastic response of a polygonal packing. Phys. Rev. E **71** (5), 051304 (2005)
3. Arthur, J.R.F., Menzies, B.K.: Inherent anisotropy in a sand. Géotechnique **22**(1), 115–128 (1972)
4. Oda, M.: Initial fabrics and their relations to mechanical properties of granular material. Soils Found. **12**(1), 18–36 (1972)
5. Azami, A., Pietruszczak, S., Guo, P.: Bearing capacity of shallow foundations in transversely isotropic granular media. Int. J. Numer. Anal. Ethods Geomech. **34**, 771–793 (2010)
6. Luding, S. : Micro-macro models for anisotropic granular media. In: Vermeer, P.A., Ehlers, W., Herrmann, H.J., Ramm, E. (eds.) Modelling of Cohesive-Frictional Materials, pp. 195–206. Balkema, Leiden, Netherlands (2004)
7. Luding, S., Perdahcıoglu, E.S.: A local constitutive model with anisotropy for various homogeneous 2D biaxial deformation modes. Chemie Ingenieur Technik **83**(5), 672–688 (2011)
8. Oda, M., Koishikawa, I., Higuchi, T.: Experimental study of anisotropic shear strength of sand by plane strain test. Soils Found. **18**(1), 26–38 (1978)
9. Tatsuoka, F., Nakamura, S., Huang, C.-C.: Strength anisotropy and shear band direction in plane strain tests of sand. Soils Found. **30**(1), 35–54 (1990)
10. Oda, M.: Anisotropic strength of cohesionless sands. J. Geotech. Eng. Div. **107**(4), 1219–1231 (1981)
11. Tatsuoka, F., Sakamoto, M., Kawamura, T., Fukushima, S.: Shear and deformation characteristics of sand in plane strain compression at extremely low pressure. Soils Found. **26**(1), 65–84 (1986)
12. Guo, P.: Modified direct shear test for anisotropic strength of sand. J. Eng. Mech. **134**(9), 1311–1318 (2008)
13. Lam, W.K., Tatsuoka, F.: Effects of initial anisotropic fabric and s_2 on strength and deformation characteristics of sand. Soils Found. **28**(1), 89–106 (1988)
14. Ochiai, H., Lade, P.V.: Three-dimensional behavior of sand with anisotropic fabric. J. Geotech. Eng. Div. **109**(10), 1313–1328 (1983)
15. Lade, P.V., Nam, J., Hong, W.P.: Shear banding and cross-anisotropic behavior observed in laboratory sand tests with stress rotation. Can. Geotech. J. **45**(1), 74–84 (2008)
16. Miura, K., Miura, S., Toki, S.: Deformation behavior of anisotropic dense sand under principal stress axes rotation. Soils Found. **26**(1), 36–52 (1986)
17. Oda, M., Konishi, J., Nemat-Nasser, S.: Experimental micromechanical evolution of strength of granular materials: effects of particle rolling. Mech. Mater. **1**, 269–283 (1982)
18. Wakabayashi, T.: Photoelastic method for determination of stress in powdered mass. In: Proceedings of 7th Japanese National Congress on Applied Mechanics 1957, pp. 153–158
19. Drescher, A.: An experimental investigation of flow rule for granular materials. Géotechnique **26**(4), 591–601 (1976)
20. Oda, M., Kazama, H., Konishi, J.: Effects of induced anisotropy on the development of shear bands in granular materials. Mech. Mater. **28**, 103–111 (1998)
21. Oda, M., Kazama, H.: Microstructure of shear bands and its relation to the mechanisms of dilatancy and failure of dense granular soils. Géotechnique **48**(4), 465–481 (1998)

22. Azema, E., Radjai, F., Peyroux, R., Saussine, G.: Force transmission in a packing of pentagonal particles. Phys. Rev. E **76**, 011301 (2007)
23. Radjai, F., Wolf, D.E., Jean, M., Moreau, J.J.: Bimodal character of stress transmission in granular packings. Phys. Rev. Lett. **80**, 61–64 (1998)
24. Silbert, L.E., Grest, G.S., Landry, J.W.: Statistics of the contact network in frictional and frictionless granular packings. Phys. Rev. E **66**, 1–9 (2002)
25. Moreau, J.J.: Numerical investigation of shear zones in granular materials. In: Wolf, D.E., Grassberger, P. (eds.) Friction, Arching, Contact Dynamics, pp. 233–247. World Scientific, Singapore (1997)
26. Cundall, P.A., Strack, O.D.L.: A discrete numerical model for granular assemblies. Géotechnique **46**(3), 529–546 (1979)
27. Ting, J.M., Meachum, L.R.: Effect of bedding plane orientation on the behavior of granular systems. Mech. Mater. Discontinuities Heterogeneities **201**, 43–57 (1995)
28. Bardet, J.P., Proubet, J.: Shear-band analysis in idealized granular material. J. Eng. Mech. **118**(2), 397–415 (1992)
29. Cundall, P.A.: TRUBAL User's guide. In: Department of Civil and Mineral Engineering. University of Minneapolis, Minnesota (1989)
30. Donzé, F., Magnier, S.A., Daudeville, L., Mariotti, C.: Formulation of a three-dimensional numerical model of brittle behavior. Geophys. J. Int. **122**, 790–802 (1995)
31. Iwashita, K., Oda, M.: Rolling resistance at contacts in simulation of shear band development by DEM. J. Eng. Mech. **124**(3), 285–292 (1998)
32. Iwashita, K., Oda, M.: Micro-deformation mechanism of shear banding process based on modified distinct element method. Powder Technol. **109**, 192–205 (2000)
33. Ni, Q., Powrie, W., Zhang, X., Harkness, R.: Effect of particle properties on soil behavior: 3-D numerical modeling of shear box tests. In: ASCE Geotechnical Special Publication No. 96, pp. 58–70. ASCE, Reston (2000)
34. Fu, P., Dafalias, Y.F.: Study of anisotropic shear strength of granular materials using DEM simulation. Int. J. Numer. Anal. Methods Geomech. **35**(10), 1098–1126 (2010)
35. Rothenburg, L., Bathurst, R.J.: Influence of particle eccentricity on micromechanical behavior of granular materials. Mech. Mater. **16**(1–2), 141–152 (1993)
36. Lin, X., Ng, T.-T.: A three-dimensional discrete element model using arrays of ellipsoids. Géotechnique **47**(2), 319–329 (1997)
37. Jensen, R.P., Bosscher, P.J., Plesha, M.E., Edil, T.B.: DEM simulation of granular media with disk clusters. Int. J. Numer. Anal. Methods Geomech. **23**(6), 531–547 (1999)
38. Sallam, A.M.: Studies on modeling angular soil particles using the discrete element method. Ph.D. dissertation, University of South Florida, USA (2004)
39. Mirghasemi, A.A., Rothenburg, L., Matyas, E.L.: Influence of particle shape on engineering properties of assemblies of two-dimensional polygon-shaped particles. Géotechnique **52**(3), 209–217 (2002)
40. Peña, A.A., Lizcano, A., Alonso-Marroquin, F., Herrmann, H.J.: Biaxial test simulations using a packing of polygonal particles. Int. J. Numer. Anal. Methods Geomech. **32**, 143–160 (2008)
41. Strack, O.D.L., Cundall, P.A.: The distinct element method as a tool for research in granular media. In: Report ENG 76-20711. National Science Foundation, Department of Civil and Mining Engineering, University of Minnesota (1978)
42. Lambe, T.W., Whitman, R.V.: Soil Mechanics. Wiley, New York (1969)
43. Rothenburg, L.: Micromechanics of idealized granular systems. Ph.D. dissertation, Carlton University (1980)
44. Christoffersen, J., Mehrabadi, M.M., Nemat-Nasser, S.: Micromechanical description of granular material behavior. J. Appl. Mech. Trans. ASME **48**(2), 339–344 (1981)
45. Bathurst, R.J.: A study of stress and anisotropy in idealized granular assemblies. Ph.D. dissertation, Queen's University (1985)
46. Seyedi Hosseininia, E., Mirghasemi, A.A.: Numerical simulation of breakage of two-dimensional polygon-shaped particles using discrete element method. Powder Technol. **166**, 100–112 (2006)
47. Peña, A.A., García-Rojo, R., Herrmann, H.J.: Influence of particle shape on sheared dense granular media. Granular Matter **9**, 279–291 (2007)
48. Mahmood, Z., Iwashita, K.: Influence of inherent anisotropy on mechanical behavior of granular materials based on DEM simulations. Int. J. Numer. Anal. Methods Geomech. **34**, 795–819 (2010)
49. Tatsuoka, F., Ochiai, H., Fujii, S., Okamoto, M.: Cyclic undrained triaxial and torsional shear strength of sands for different sample preparation methods. Soils Found. **26**, 23–41 (1986)
50. Horn, H.M., Deere, D.U.: Frictional characteristics of minerals. Géotechnique **12**, 319–335 (1962)
51. Sazzad, M.M., Suzuki, K.: Micromechanical behavior of granular materials with inherent anisotropy under cyclic loading using 2D DEM. Granular Matter **12**, 597–605 (2010)
52. Houlubec, I., D'Appolonia, E.: Effect of particle shape on the engineering properties of granular soils. In: Proceedings of Symposium on Evaluation of Relative Density, Los Angeles 1973. ASTM STP 523, pp. 304–318
53. Santamarina, J.C., Cho, G.C.: Soil behaviour: the role of particle shape. In: Proceedings Skempton Conference, London (March 2004)
54. Nouguier-Lehon, C., Cambou, B., Vincens, E.: Influence of particle shape and angularity on the behaviour of granular materials: a numerical analysis. Int. J. Numer. Anal. Methods Geomech. **27**, 1207–1226 (2003)
55. Azema, E., Radja, F., Peyroux, R., Saussine, G. (2009) Influence of particle shape on shear stress in granular media. In: Appert-Rolland, C., Chevoir, F., Gondret, P., Lassarre, S., Lebacque, J.-P., Schreckenberg, M. (eds.) Traffic and Granular Flow'07, pp. 497–505. Springer
56. Oda, M., Nemat-Naser, S., Konishi, J.: Stress-induced anisotropy in granular masses. Soils Found. **25**(3), 85–97 (1985)
57. Peters, J.F., Muthuswamy, M., Wibowo, J., Tordesillas, A.: Characterization of force chains in granular material. Phys. Rev. E **72**(4), 041307 (2005)
58. Sanfratello, L., Zhang, J., Cartee, S., Fukushima, E.: Exponential distribution of force chain lengths: a useful statistic that characterizes granular assemblies. Granular Matter **13**(5), 511–516
59. Tordesillas, A., Walker, D.M., Lin, Q.: Force cycles and force chains. Phys. Rev. E **81**(1), 011302 (2010)
60. Rothenburg, L., Bathurst, R.J.: Analytical study of induced anisotropy in idealized granular materials. Géotechnique **39**(4), 601–614 (1989)